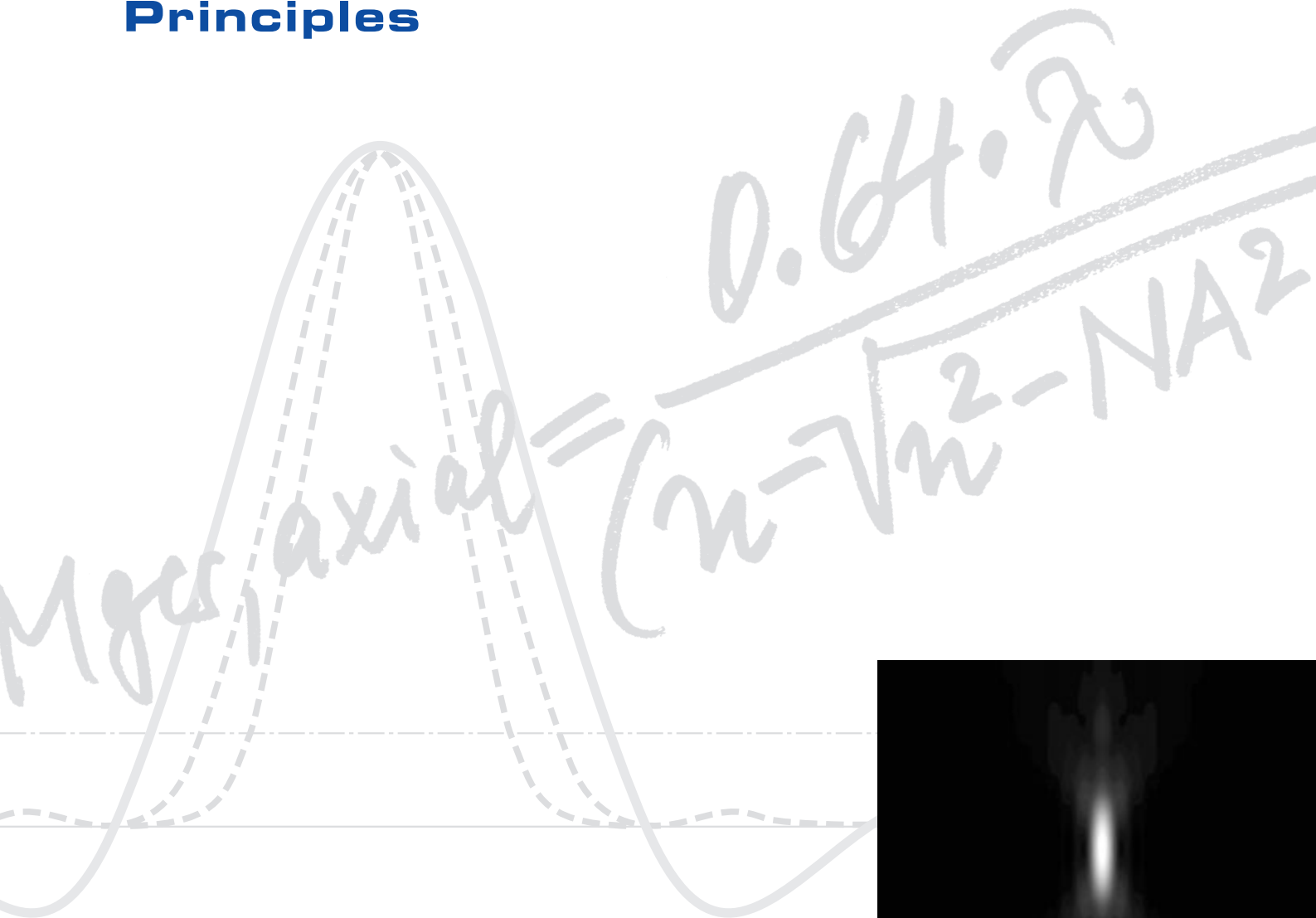


# Confocal Laser Scanning Microscopy

## Principles



**Optical Image Formation**  
**Electronic Signal Processing**  
**Authors/Sources/References**



# Contents

Page

Introduction.....	2
<b>Part I: Optical Image Formation</b>	
1. The Point Spread Function.....	7
2. Resolution and Depth Discrimination in a Confocal LSM .....	9
2.1 Geometric-optical confocality .....	11
2.1.1 Resolution .....	11
2.1.2 Depth discrimination .....	11
2.2 Wave-optical confocality .....	12
<b>Part II Electronic Signal Processing</b>	
1. Introduction .....	17
2. Digitization / Signal Processing .....	17
3. Noise.....	22
3.1 Resolution and shot noise - resolution probability .....	24
3.2 Possibilities to improve SNR .....	26
4. Summary .....	27
<b>Part III: Authors / Sources / References.....</b>	<b>28</b>
<b>Appendix: Poster 'The Confocal Laser Scanning Microscope' Overview</b>	

# Introduction

In recent years, the confocal laser scanning microscope (LSM) has become widely established as a research instrument.

LSM applications in biology and medicine predominantly employ fluorescence, but it is also possible to use the transmission mode with conventional contrasting methods, such as differential interference contrast (DIC), as well as to overlay the transmission and confocal fluorescence images of the same specimen area.

Another important field of application is materials science, where the LSM is used especially in the reflection mode and with such methods as polarization.

Confocal microscopes are even used in routine quality inspection in industry. Here, confocal images provide an efficient way to detect defects in semiconductor circuits.

The present brochure aims at giving a scientifically sound survey of the special nature of image formation in a confocal LSM.

Following a description of the fundamental differences between a conventional and a confocal microscope, the article will set out the special features of the confocal LSM and the capabilities resulting from them.

The conditions in fluorescence applications will be given priority treatment throughout.

## Image generation

The complete generation of the two-dimensional object information from the focal plane (object plane) of a confocal LSM essentially comprises three process steps:

1. Line-by-line scanning of the specimen with a focused laser beam deflected in the X and Y directions by means of two galvanometric scanners.
2. Pixel-by-pixel detection of the fluorescence emitted by the scanned specimen details, by means of a photomultiplier (PMT).

3. Digitization of the object information contained in the electrical signal provided by the PMT (for presentation, the image data are issued, pixel by pixel, from a digital matrix memory to a monitor screen).

Figure 1 schematically shows the factors of influence on image formation in a confocal LSM.

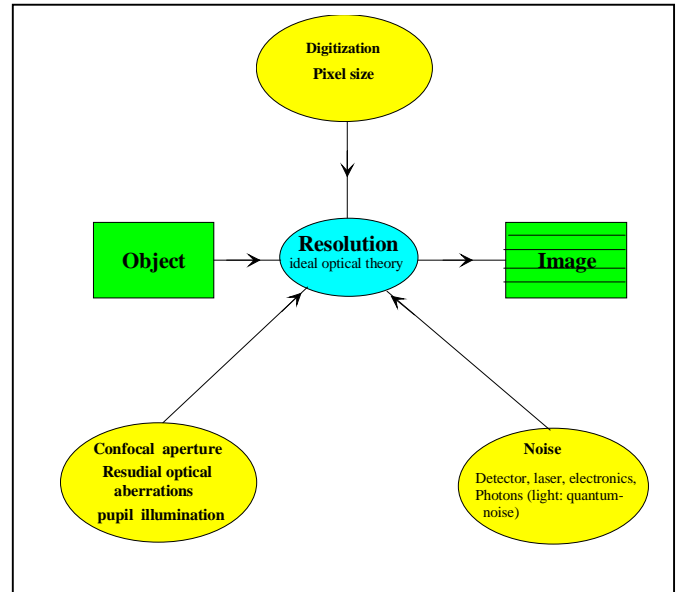


*Fig. 1 The quality of the image generated in a confocal LSM is not only influenced by the optics (as in a conventional microscope), but also, e.g., by the confocal aperture (pinhole) and by the digitization of the object information (pixel size). Another important factor is light noise (laser noise, or the shot noise of the fluorescent light). To minimize noise, signal-processing optoelectronic and electronic devices also need to be optimized.*

## Scanning Process

In a conventional light microscope, object-to-image transformation takes place simultaneously and parallel for all object points. By contrast, the specimen in a confocal LSM is irradiated in a pointwise fashion, i.e. serially, and the physical interaction between the laser light and the specimen detail irradiated (e.g. fluorescence) is measured point by point as well. To obtain information about the entire specimen, it is necessary to guide the laser beam across the specimen, or to move the specimen relative to the laser beam, a process known as scanning. Accordingly, confocal systems are also known as point-probing scanners.

To obtain images of microscopic resolution from a confocal LSM, a computer and dedicated software are indispensable.

The descriptions below exclusively cover the point scanner principle as implemented, for example, in Carl Zeiss laser scanning microscopes. Configurations in which several object points are irradiated simultaneously are left out of consideration.

## Confocal beam path

The decisive design feature of a confocal LSM compared with a conventional microscope is the confocal aperture (usually called pinhole) arranged in a plane conjugate to the intermediate image plane and, thus, to the object plane of the microscope. As a result, the detector (PMT) can only detect light that has passed the pinhole. The pinhole diameter is variable; ideally, it is infinitely small, and thus the detector looks at a point (point detection). As the laser beam is focused to a diffraction-limited spot, which illuminates only a point of the object at a time, the point illuminated and the point observed (i.e. image and object points) are situated in conjugate planes, i.e. they are focused onto each other. The result is what is called a confocal beam path (see Figure 2).

## Pinhole

Depending on the diameter of the pinhole light coming from object points outside the focal plane is more or less obstructed and thus excluded from detection. As the corresponding object areas are invisible in the image, the confocal microscope can be understood as an inherently depth-discriminating optical system.

By varying the pinhole diameter, the degree of confocality can be adapted to practical requirements. With the aperture fully open, the image is non-confocal. As an added advantage, the pinhole suppresses stray light, which improves image contrast.

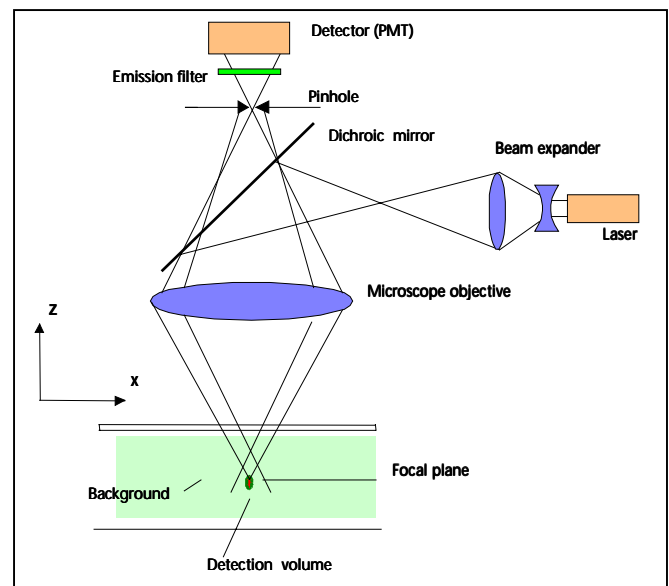


*Fig. 2 Beam path in a confocal LSM. A microscope objective is used to focus a laser beam onto the specimen, where it excites fluorescence, for example. The fluorescent radiation is collected by the objective and efficiently directed onto the detector via a dichroic beamsplitter. The interesting wavelength range of the fluorescence spectrum is selected by an emission filter, which also acts as a barrier blocking the excitation laser line. The pinhole is arranged in front of the detector, on a plane conjugate to the focal plane of the objective. Light coming from planes above or below the focal plane is out of focus when it hits the pinhole, so most of it cannot pass the pinhole and therefore does not contribute to form the image.*

## Optical Slices

With a confocal LSM it is therefore possible to exclusively image a thin "optical slice" out of a "thick" specimen (typically, up to 100  $\mu\text{m}$ ), a method known as optical sectioning. Under suitable conditions, the thickness (Z dimension) of such a slice may be less than 500 nm.

The fundamental advantage of the confocal LSM over a conventional microscope is obvious: In conventional fluorescence microscopy, the image of a "thick" biological specimen will only be in focus if its Z dimension is not greater than the wave-optical depth of focus specified for the respective objective.

Unless this condition is satisfied, the in-focus image information from the object plane of interest is mixed with out-of focus image information from planes outside the focal plane. This reduces image contrast and increases the share of stray light detected. If multiple fluorescences are observed, there will in addition be a color mix of the image information obtained from the channels involved (see Figure 3, top).

A confocal LSM can therefore be used to advantage especially where "thick" specimens (such as biological cells in tissue) have to be examined by fluorescence. The possibility of optical sectioning eliminates the drawbacks attached to the observation of such specimens by conventional fluorescence microscopy. With multicolor fluorescence, the various channels are satisfactorily separated and can be recorded simultaneously<sup>1</sup>.

With regard to reflective specimens, the main application is the investigation of the topography of 3D surface textures.

Figure 3 demonstrates the capability of a confocal LSM by a comparison of the confocal and non-confocal images of a triple-labeled aggregate of cells (mouse intestine section).

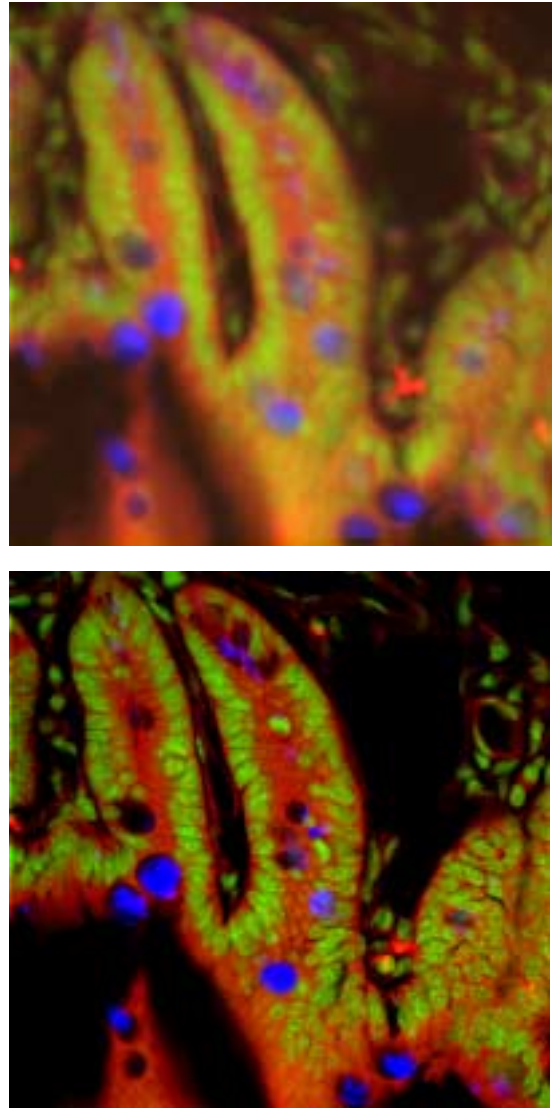


*Fig. 3 Non-confocal (top) and confocal (bottom) image of a triple-labeled cell aggregate (mouse intestine section). In the non-confocal image, specimen planes outside the focal plane degrade the information of interest from the focal plane, and differently stained specimen details appear in mixed color. In the confocal image (bottom), specimen details blurred in non-confocal imaging become distinctly visible, and the image throughout is greatly improved in contrast.*

---

<sup>1</sup> See also such methods as multitracking, in which the channels in the overall image appear completely separated thanks to their sequential recording (no 'crosstalk').

### 3<sup>rd</sup> dimension

In addition to the possibility to observe a single plane (or slice) of a "thick" specimen in good contrast, optical sectioning allows a great number of slices to be cut and recorded at different planes of the specimen, with the specimen being moved along the optical axis (Z) by controlled increments. The result is a 3D data set, which provides information about the spatial structure of the object. The quality and accuracy of this information depend on the thickness of the slice and on the spacing between successive slices (optimum scanning rate in Z direction = 0.5x the slice thickness). By computation, various aspects of the object can be generated from the 3D data set (3D reconstruction, sections of any spatial orientation, stereo pairs etc.). Figure 4 shows an example of a 3D data set and a 3D reconstruction computed from it.

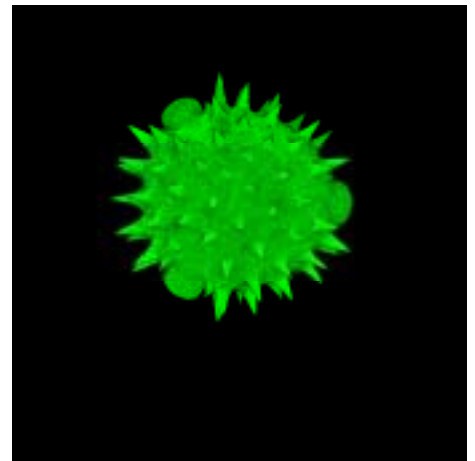
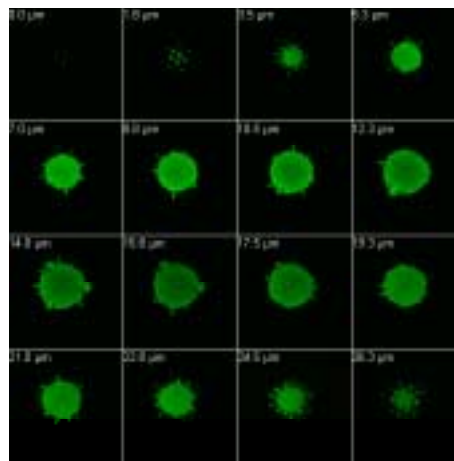
### Time series

A field of growing importance is the investigation of living specimens that show dynamic changes even in the range of microseconds. Here, the acquisition of time resolved confocal image series (known as time series) provides a possibility of visualizing and quantifying the changes.

The following section (Part I) deals with the purely optical conditions in a confocal LSM and the influence of the pin-hole on image formation. From this ideal values for resolution and optical slice thickness are derived. Part II relativizes the ideal conditions by looking at the digitizing process and the noise introduced by the light as well as by the optoelectronic components of the system.

The table on page 14 provides a summary of the essential results of Part I. A schematic overview of the entire content and its practical relevance is given on the fold-out back pages.

*Fig. 4 Left: A representative set of sections of the 3D data set of a pollen grain (autofluorescence). Originally, the data set contains 116 images. The slices are 250 nm apart. The object information is clearly seen to vary with the Z position.  
Right: Projection enhancing the 3D structure, generated from the data set by computation.*





# Optical Image Formation

## 1. The Point Spread Function

In order to understand the optical performance characteristics of a confocal LSM in detail, it is necessary to have a closer look at the fundamental optical phenomena resulting from the geometry of the confocal beam path. As mentioned before, what is most essential about a confocal LSM is that both illumination and observation (detection) are limited to a point.

Not even an optical system of diffraction-limited design can image a truly point-like object as a point. The image of an ideal point object will always be somewhat blurred, or "spread" corresponding to the imaging properties of the optical system. The image of a point can be described in quantitative terms by the point spread function (PSF), which maps the intensity distribution in the image space. Where the three-dimensional imaging properties of a confocal LSM are concerned, it is necessary to consider the 3D image or the 3D-PSF.

In the ideal, diffraction-limited case (no optical aberrations, homogeneous illumination of the pupil - see *InfoBox "Pupil Illumination"*), the 3D-PSF is of comet-like, rotationally symmetrical shape.

Actually, however, any optical system has residual aberrations. Essentially, these cause deviations from the rotational symmetry of the 3D-PSF. The width of the 3D-PSF (resolution) is determined, apart from other factors (see section 2.1.1), by the expansion of the laser beam relative to the diameter of the objective's pupil (degree of homogeneity of pupil illumination). Moreover, the expansion leads to a vignetting of the beam at the objective pupil, so that the energy quantity transported into the object is reduced (see *InfoBox "Pupil Illumination"*).

But, as the laser is a high-energy light source, it is possible to obtain near-optimum resolving properties and, simultaneously, a sufficient energy density at the focus of the microscope objective. If, in addition, the residual aberrations can be minimized, the case of diffraction-limited imaging in a confocal LSM is largely met.

For illustration, Figure 5 shows two-dimensional sections (XZ and XY) through an ideal 3D-PSF.

From the illustration it is evident that the central maximum of the 3D-PSF, in which 86.5 % of the total energy available in the pupil are concentrated, can be described as an ellipsoid of rotation. For considerations of resolution and optical slice thickness it is useful to define the half-maximum area of the ellipsoid of rotation, i.e. the well-defined area in which the intensity of the 3D point image in axial and lateral directions has dropped to half of the central maximum.

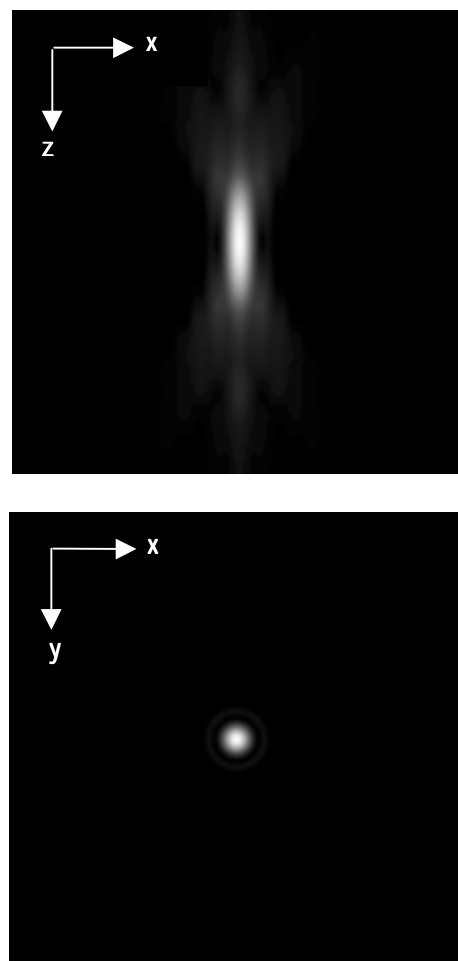


*Fig.5 Section through the 3D-PSF in Z direction – top and in XY-direction – bottom (computed; dimensionless representation); the central, elliptical maximum is distinctly visible. The Airy disk (central maximum in the bottom illustration) is contained in the 3D-PSF as the greatest core diameter in lateral direction.*

## Pupil Illumination

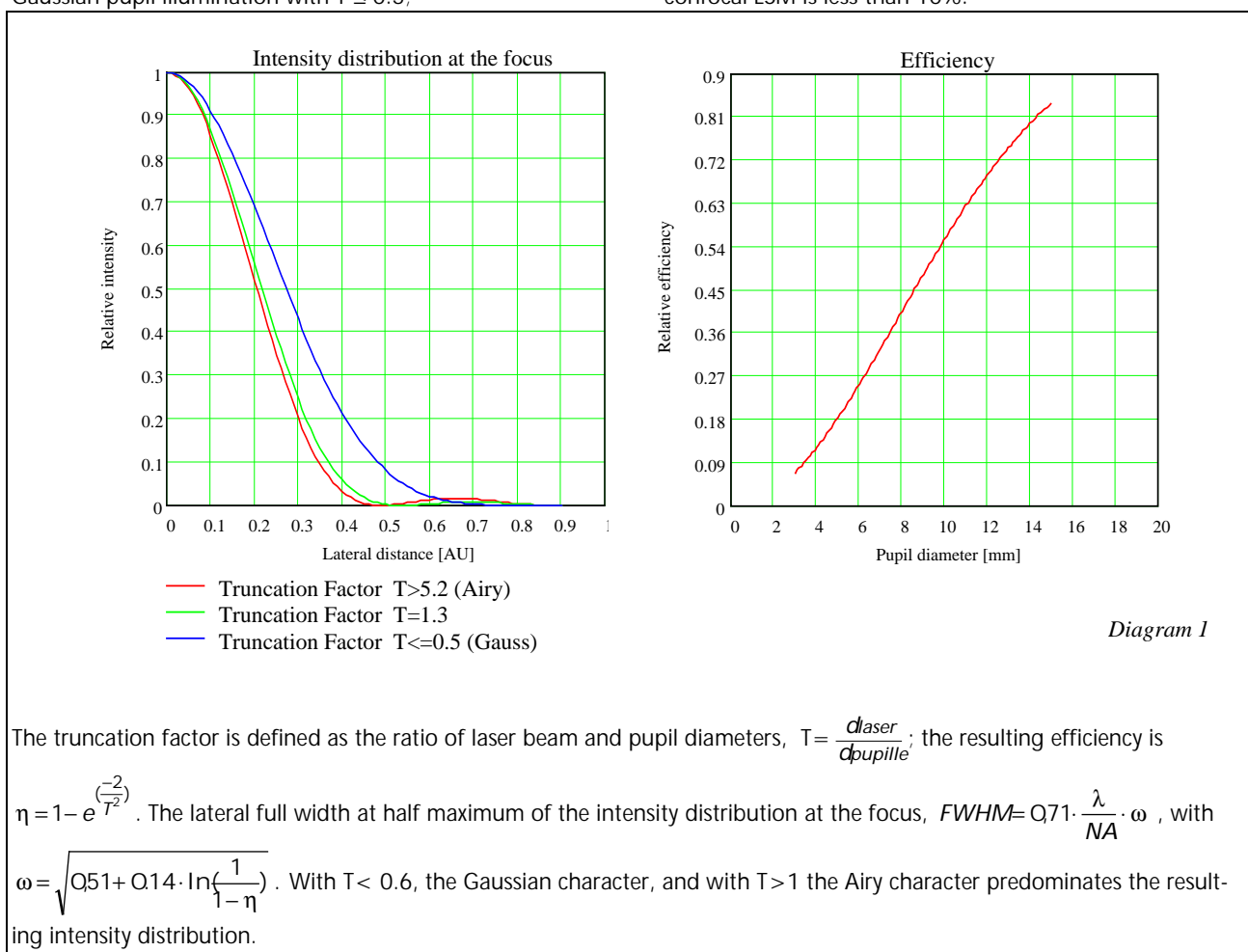
All descriptions in this monograph suggest a confocal LSM with a ray geometry providing homogeneous illumination at all lens cross sections. The focus generated in the object has an Airy distribution, being a Fourier transform of the intensity distribution in the objective's pupil plane. However, the truncation of the illuminating beam cross-section needed for an Airy distribution causes a certain energy loss (a decrease in efficiency). [In Carl Zeiss microscope objectives, the pupil diameter is implemented by a physical aperture close to the mounting surface].

The Airy distribution is characterized by a smaller width at half maximum and a higher resolving power. Diagram 1 (see at bottom left) shows the intensity distribution at the focus as a function of the truncation factor T (the ratio of laser beam diameter ( $1/e^2$ ) and pupil diameter).

The graph presents the relative intensity distributions at the focus (each normalized to 1) for different truncation factors. (The red curve results at a homogeneous pupil illumination with  $T > 5.2$ , while the blue one is obtained at a Gaussian pupil illumination with  $T \leq 0.5$ ;

the green curve corresponds to a truncation factor  $T=1.3$ ). The lateral coordinate is normalized in Airy units (AU).

From  $T = 3$ , the Airy character is predominating to a degree that a further increase in the truncation factor no longer produces a gain in resolution. (Because of the symmetry of the point image in case of diffraction-limited imaging, the graph only shows the intensity curve in the + X direction). Diagram 2 (see at bottom right) shows the percentage efficiency as a function of pupil diameter in mm, with constant laser beam expansion. The smaller the pupil diameter, the higher the T-factor, and the higher the energy loss (i.e. the smaller the efficiency). Example: If the objective utilizes 50% of the illuminating energy supplied, this means about 8% resolution loss compared to the ideal Airy distribution. Reducing the resolution loss to 5% is penalized by a loss of 70% of the illuminating energy. In practice, the aim is to reach an optimal approximation to a homogeneous pupil illumination; this is one reason for the fact that the efficiency of the excitation beam path in a confocal LSM is less than 10%.



Any reference to the PSF in the following exclusively refers to the half-maximum area. Quantitatively the half-maximum area is described in terms of the full width at half maximum (FWHM), a lateral or axial distance corresponding to a 50% drop in intensity.

The total PSF ( $PSF_{tot}$ ) of a confocal microscope behind the pinhole is composed of the PSFs of the illuminating beam path ( $PSF_{ill}$ ; point illumination) and the detection beam path ( $PSF_{det}$ ; point detection). Accordingly, the confocal LSM system as a whole generates two point images: one by projecting a point light source into the object space, the other by projecting a point detail of the object into the image space. Mathematically, this relationship can be described as follows:

$$PSF_{tot}(x, y, z) = PSF_{ill}(x, y, z) \cdot PSF_{det}(x, y, z) \quad (1)$$

$PSF_{ill}$  corresponds to the light distribution of the laser spot that scans the object. Its size is mainly a function of the laser wavelength and the numerical aperture of the microscope objective. It is also influenced by diffraction at the objective pupil (as a function of pupil illumination) and the aberrations of all optical components integrated in the system. [Note: In general, these aberrations are low, having been minimized during system design]. Moreover,  $PSF_{ill}$  may get deformed if the laser focus enters thick and light-scattering specimens, especially if the refractive indices of immersion liquid and mounting medium are not matched and/or if the laser focus is at a great depth below the specimen surface (see [8]).

$PSF_{det}$  is also influenced by all these factors and, additionally, by the pinhole size. For reasons of beam path efficiency (see Part II), the pinhole is never truly a point of infinitely small size and thus  $PSF_{det}$  is never smaller in dimension than  $PSF_{ill}$ . It gets evident, that the imaging properties of a confocal LSM are determined by the interaction between  $PSF_{ill}$  and  $PSF_{det}$ . As a consequence of the interaction process,  $PSF_{tot} \leq PSF_{ill}$ .

With the pinhole diameter being variable, the effects obtained with small and big pinhole diameters must be expected to differ.

In the following sections, various system states are treated in quantitative terms.

From the explanations made so far, it can also be derived that the optical slice is not a sharply delimited body. It does not start abruptly at a certain Z position, nor does it end abruptly at another. Because of the intensity distribution along the optical axis, there is a continuous transition from object information suppressed and such made visible. Accordingly, the out-of-focus object information actually suppressed by the pinhole also depends on the correct setting of the image processing parameters (PMT high voltage, contrast setting). Signal overdrive or excessive off-set should be avoided.

## 2. Resolution and Depth Discrimination in a Confocal LSM

Wherever quantitative data on the resolving power and depth discrimination of a confocal LSM are specified, it is necessary to distinguish clearly whether the objects they refer to are point-like or extended, and whether they are reflective or fluorescent. These differences involve distinctly differing imaging properties. Fine structures in real biological specimens are mainly of a filiform or point-like fluorescent type, so that the explanations below shall be limited to point-like fluorescent objects. The statements made for this case are well applicable to practical assignments. As already mentioned, the pinhole diameter plays a decisive role in resolution and depth discrimination. With a pinhole diameter greater than 1 AU (AU = Airy unit – see *InfoBox "Optical Coordinates"*), the depth discriminating properties under consideration are essentially based on the law of geometric optics (geometric-optical confocality). The smaller the pinhole diameter, the more  $PSF_{det}$  approaches the order of magnitude of  $PSF_{ill}$ . In the limit case ( $PH < 0.25$  AU), both PSFs are approximately equal in size, and wave-optical image formation laws clearly dominate (wave-optical confocality).

Figure 6 illustrates these concepts. It is a schematic representation of the half-intensity areas of  $PSF_{ill}$  and  $PSF_{det}$  at selected pinhole diameters.

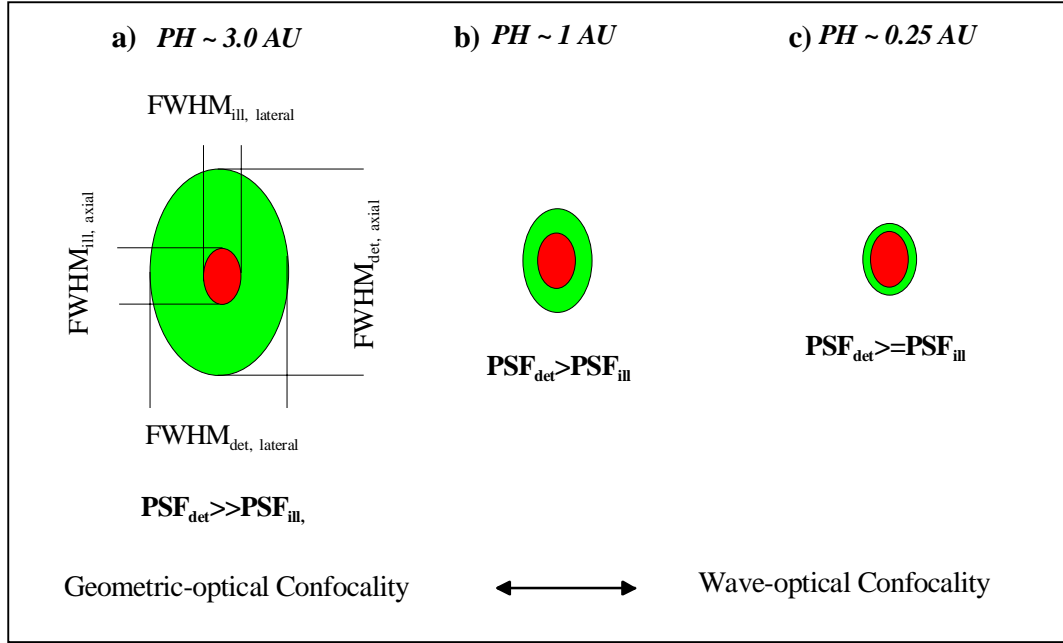


Fig. 6 Geometric-optical (a) and wave-optical confocality (c) [XZ view]. The pinhole diameter decreases from (a) to (c). Accordingly,  $PSF_{det}$  shrinks until it approaches the order of magnitude of  $PSF_{ill}$  (c).

Depending on the pinhole size ( $PSF_{det}$ ), a distinction should be made between geometric-optical and wave-optical confocality. Depending on which kind of confocality dominates, the data and computation methods for resolution

and depth discrimination differ. A comparison with image formation in conventional microscopes is interesting as well. The following sections deal with this in detail.

### InfoBox

## Optical Coordinates

In order to enable a representation of lateral and axial quantities independent of the objective used, let us introduce optical coordinates oriented to microscopic imaging. Given the imaging conditions in a confocal microscope, it suggests itself to express all lateral sizes as multiples of the Airy disk diameter. Accordingly, the Airy unit (AU) is defined as:

$$1 \text{ AE} = \frac{1.22 \cdot \lambda}{NA}$$

$NA$  = numerical aperture of the objective

$\lambda$  = wavelength of the illuminating laser light

with  $NA = 1.3$  and  $\lambda = 488 \text{ nm} \rightarrow 1 \text{ AE} = 0.458 \mu\text{m}$

The Airy unit is primarily used for normalizing the pinhole diameter.

Thus, when converting a given pinhole diameter into AUs, we need to consider the system's total magnification; which means that the Airy disk is projected onto the plane of the pinhole (or *vice versa*).

Analogously, a sensible way of normalization in the axial direction is in terms of multiples of the wave-optical depth of field. Proceeding from the Rayleigh criterion, the following expression is known as Rayleigh unit (RU):

$$1 \text{ RE} = \frac{n \cdot \lambda}{NA^2}$$

$n$  = refractive index of immersion liquid

with  $NA = 1.3$ ,  $\lambda = 488 \text{ nm}$  and  $n = 1.52 \rightarrow 1 \text{ RE} = 0.439 \mu\text{m}$

The Rayleigh unit is used primarily for a generally valid representation of the optical slice thickness in a confocal LSM - see also diagram 2.

## 2.1 Geometric-optical confocality

### 2.1.1 Resolution

Resolution, in case of large pinhole diameters ( $PH > 1AU$ ), is meant to express the separate visibility, both laterally and axially, of points during the scanning process. Imagine an object consisting of individual points: all points spaced closer than the extension of  $PSF_{III}$  are blurred (spread), i.e. they are not resolved.

Quantitatively, resolution results from the axial and lateral extension of the scanned laser spot, or the elliptical half-intensity area of  $PSF_{III}$ . On the assumption of homogeneous pupil illumination, the following equations apply:

Axial:

$$FWHM_{ill,axial} = \frac{0.88 \cdot \lambda_{exc}}{(n - \sqrt{n^2 - NA^2})} \quad (2)$$

$n$  = refractive index of immersion liquid,  $NA$  = numerical aperture of the microscope objective,  $\lambda_{exc}$  = wavelength of the excitation light

If  $NA < 0.5$ , equation (2) can be approximated by:

$$\approx \frac{1.67 \cdot n \cdot \lambda_{exc}}{NA^2} \quad (2a)$$

Lateral:

$$FWHM_{ill,lateral} = 0.51 \frac{\lambda_{exc}}{NA} \quad (3)$$

At first glance, equations (2a) and (3) are not different from those known for conventional imaging (see [3]). It is striking, however, that the resolving power in the confocal microscope depends only on the wavelength of the illuminating light, rather than exclusively on the emission wavelength as in the conventional case.

Compared to the conventional fluorescence microscope, confocal fluorescence with large pinhole diameters leads to a gain in resolution by the factor  $(\lambda_{em}/\lambda_{exc})$  via the Stokes shift.

### 2.1.2 Depth discrimination

Optical slice thickness (depth discrimination) and stray light suppression (contrast improvement) are basic properties of a confocal LSM, even if the pinhole diameter is not an ideal point (i.e. not infinitely small). In this case, both depth discrimination and stray light suppression are determined exclusively by  $PSF_{det}$ . This alone brings an improvement in the separate visibility of object details over the conventional microscope.

Hence, the diameter of the corresponding half-intensity area and thus the optical slice thickness is given by:

$$FWHM_{det,axial} = \sqrt{\left(\frac{0.88 \cdot \lambda_{em}}{n - \sqrt{n^2 - NA^2}}\right)^2 + \left(\frac{\sqrt{2} \cdot n \cdot PH}{NA}\right)^2} \quad (4)$$

$\lambda_{em}$  = emission wavelength  
 $PH$  = object-side pinhole diameter [ $\mu m$ ]  
 $n$  = refractive index of immersion liquid  
 $NA$  = numerical aperture of the objective

Equation (4) shows that the optical slice thickness comprises a geometric-optical and a wave-optical term. The wave-optical term (first term under the root) is of constant value for a given objective and a given emission wavelength. The geometric-optical term (second term under the root) is dominant; for a given objective it is influenced exclusively by the pinhole diameter.

Likewise, in the case of geometric-optical confocality, there is a linear relationship between depth discrimination and pinhole diameter. As the pinhole diameter is constricted, depth discrimination improves (i.e. the optical slice thickness decreases).

Diagram 2, a graphical representation of equation (4), illustrates this fundamental relation. The graph shows the geometric-optical term alone (blue line) and the curve resulting from eq. 4 (red line). The difference between the two curves is a consequence of the wave-optical term.

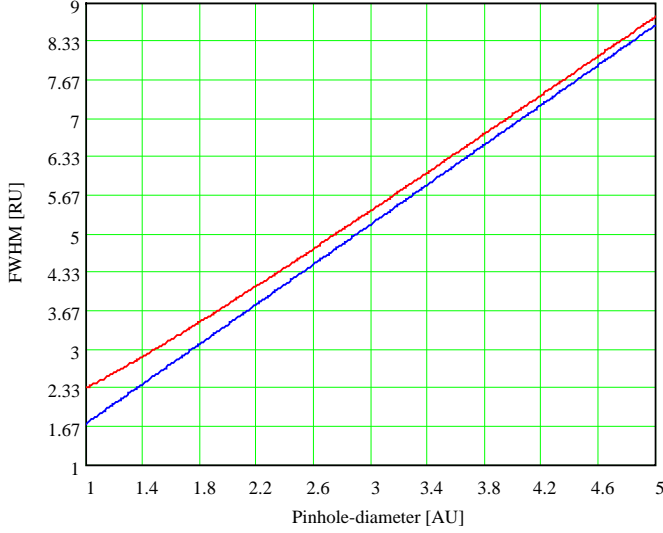


Diagram 2 Axial optical slice thickness as a function of the pinhole diameter (red line). Parameters:  $NA = 0.6$ ;  $n = 1$ ;  $\lambda = 520 \text{ nm}$ . The X axis is dimensioned in Airy units, the Y axis (slice thickness) in Rayleigh units (see also: InfoBox "Optical Coordinates"). In addition, the geometric-optical term in equation 4 is shown separately (blue line) – see also diagram 4a

Above a pinhole diameter of about 1.5 AU, the influence of diffraction effects is nearly constant.

The interaction between  $PSF_{III}$  and  $PSF_{det}$  mentioned in chapter 1 becomes manifest only with pinhole diameters smaller than 1 AU. For pinholes greater than 1 AU, equation (4) is a good approximation to describe the depth discrimination in a confocal LSM.

Let it be emphasized that in this case the diameters of the half-intensity areas of  $PSF_{det}$  allow no statement about the separate visibility of points (object details) in axial and lateral direction.

Thus a large diameter pinhole has no direct influence on the resolution properties of a confocal LSM. In the region of the optical section ( $FWHM_{det,axial}$ ), object details are resolved (imaged separately) only unless they are spaced not closer than described by equations (2) / (2a) / (3).

## 2.2 Wave-optical confocality

If the pinhole is closed down to a diameter of  $< 0.25 \text{ AU}$  (virtually "infinitely small"), the character of the image changes. Additional diffraction effects at the pinhole have to be taken into account, and  $PSF_{det}$  (optical slice thickness) shrinks to the order of magnitude of  $PSF_{III}$  (Z resolution) (see also Figure 6c).

In order to achieve simple formulae for the range of smallest pinhole diameters, it is practical to regard the limit case of  $PH = 0$  at first, even though it is of no practical use. In this case,  $PSF_{det}$  and  $PSF_{III}$  are identical.

The total PSF

$$PSF_{tot}(x, y, z) = (PSF_{III}(x, y, z))^2 \quad (5)$$

In fluorescence applications it is furthermore necessary to consider both the excitation wavelength  $\lambda_{exc}$  and the emission wavelength  $\lambda_{em}$ . This is done by specifying a mean wavelength <sup>2</sup>:

$$\bar{\lambda} \approx \sqrt{2} \frac{\lambda_{em} \cdot \lambda_{exc}}{\sqrt{\lambda_{exc}^2 + \lambda_{em}^2}} \quad (6)$$

Thus, equations (2) and (3) for the widths of the axial and lateral half-intensity areas are transformed into:

Axial <sup>3</sup>:

$$FWHM_{tot,axial} = \frac{0.64 \cdot \bar{\lambda}}{(n - \sqrt{n^2 - NA^2})} \quad (7)$$

If  $NA < 0.5$ , equation (7) can be approximated by

$$\approx \frac{1.28 \cdot n \cdot \bar{\lambda}}{NA^2} \quad (7a)$$

Lateral:

$$FWHM_{tot,lateral} = 0.37 \frac{\bar{\lambda}}{NA} \quad (8)$$

<sup>2</sup> For rough estimates, the expression  $\bar{\lambda} \approx \sqrt{\lambda_{em} \cdot \lambda_{exc}}$  suffices.

<sup>3</sup> It is not possible to transform eq. (4) into eq. (7) by forming a limit ( $PH \rightarrow 0$ ).

[Note: With the object being a mirror (which is often used for test purposes), the factor in equation 7 is 0.45 (instead of 0.64), and 0.88 (instead of 1.28) in equation 7a. For a fluorescent plane of finite thickness, a factor of 0.7 can be used in equation 7. This makes it clear that apart from the factors influencing the optical slice thickness, the type of specimen also affects the measurement result.]

From equations (7) and (7a) it is evident that depth resolution varies linearly with the refractive index  $n$  of the immersion liquid and with the square of the inverse value of the angular aperture  $\{ NA = n \cdot \sin(\alpha) \}$  of the objective. To achieve high depth resolution, it is important, above all, to use objectives with the highest possible angular aperture (i.e. with a high NA).

As an  $NA > 1$  can only be obtained with an immersion liquid, confocal fluorescence microscopy is usually performed with immersion objectives (see also diagram 4). A comparison with the results stated in section 2.1 shows that axial and lateral resolution in the limit case of  $PH=0$  can be improved by a factor of 1.4.

Furthermore it should be noted that, because of the wave-optical relationships discussed, the optical performance of a confocal LSM cannot be enhanced infinitely. Equations (7) and (8) supply the minimum possible slice thickness and the best possible resolution, respectively.

From the applicational point of view, the case of strictly wave-optical confocality ( $PH=0$ ) is irrelevant (see also Part II).

By merely changing the factors in equations (7) and (8) it is possible, though, to transfer the equations derived for  $PH=0$  to the pinhole diameter range up to 1 AU, to a good approximation.. The factors applicable to particular pinhole diameters can be taken from diagram 3.

It must also be noted that with  $PH < 1$  AU, a distinction between optical slice thickness and resolution can no longer be made. The thickness of the optical slice at the same time specifies the resolution properties of the system. That is why in the literature the term of depth resolution is frequently used as a synonym for depth discrimination or optical slice thickness. However, this is only correct for pinhole diameters smaller than 1 AU.

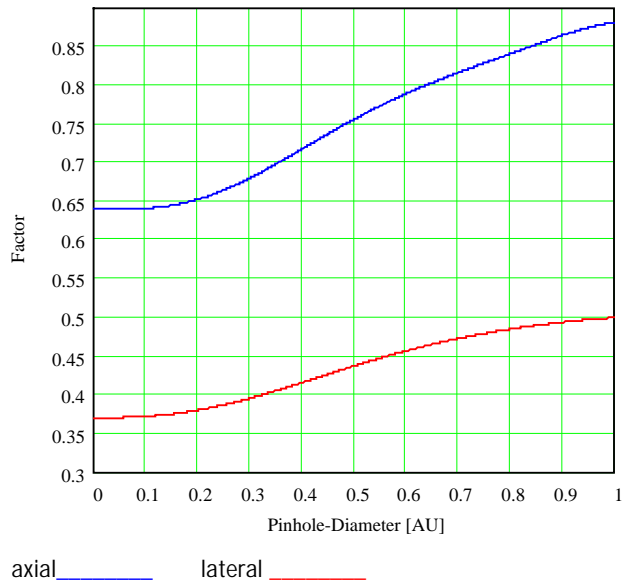


Diagram 3  
Theoretical factors for equations (7) and (8), with pinhole diameters between 0 and 1 AU.

To conclude the observations about resolution and depth discrimination (or depth resolution), Table 1 provides an overview of the formulary relationships developed in Part I. In addition, diagram 4a on page 15 shows the overall curve of optical slice thickness for a microscope objective of  $NA = 1.4$  and  $n = 1.52$  ( $\lambda = 488$  nm).

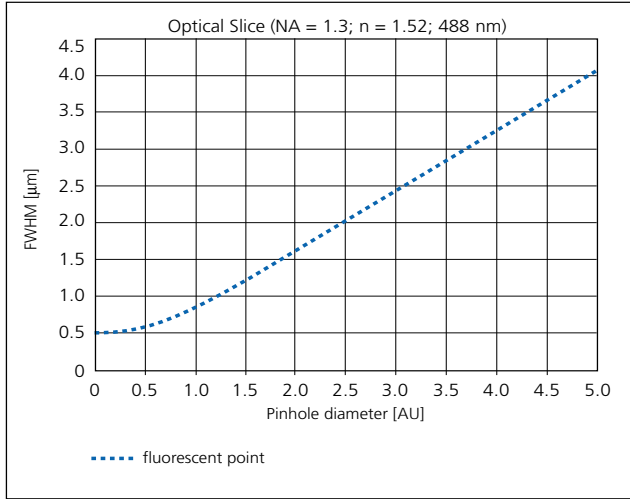
In diagrams 4 b-d, equation (7) is plotted for different objects and varied parameters ( $NA, \lambda, n$ ).

**Table 1**

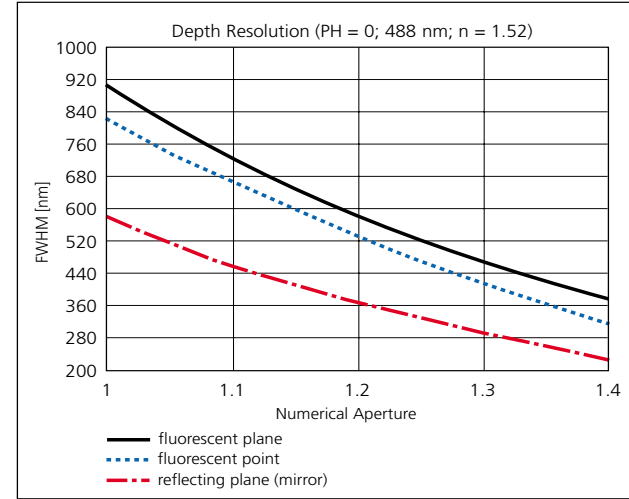
Conventional microscopy	Confocal microscopy 1 AU < PH < ∞	Confocal microscopy PH < 0.25 AU
<p>1. Optical slice thickness <b>not definable</b></p> <p>With a conventional microscope, unlike in confocal microscopy, sharply defined images of "thick" biological specimens can only be obtained if their Z dimension is not greater than the wave-optical depth of field specified for the objective used. Depending on specimen thickness, object information from the focal plane is mixed with blurred information from out-of-focus object zones.</p> <p>Optical sectioning is not possible; consequently, no formula for optical slice thickness can be given.</p>	<p>1. Optical slice thickness<sup>1)</sup></p> $\sqrt{\left(\frac{0.88 \lambda_{em}}{n - \sqrt{n^2 - NA^2}}\right)^2 + \left(\frac{\sqrt{2} \cdot n \cdot PH}{NA}\right)^2}$ <p>Corresponds to the FWHM of the intensity distribution behind the pinhole (PSF<sub>det</sub>). The FWHM results from the emission-side diffraction pattern and the geometric-optical effect of the pinhole. Here, PH is the variable object-side pinhole diameter in μm.</p>	<p>1. Optical slice thickness</p> $\frac{0.64 \bar{\lambda}}{(n - \sqrt{n^2 - NA^2})}$ <p>The term results as the FWHM of the total PSF – the pinhole acts according to wave optics.  <math>\bar{\lambda}</math> stands for a mean wavelength - see the text body above for the exact definition.  The factor 0.64 applies only to a fluorescent point object.</p>
<p>2. Axial resolution (wave-optical depth of field)</p> $\frac{n \cdot \lambda_{em}}{NA^2}$ <p>Corresponds to the width of the emission-side diffraction pattern at 80% of the maximum intensity, referred to the object plane. In the literature, the wave-optical depth of field in a conventional microscope is sometimes termed depth resolution. However, a clear distinction should be made between the terms resolution and depth resolution.</p>	<p>2. Axial resolution</p> $\frac{0.88 \lambda_{exc}}{(n - \sqrt{n^2 - NA^2})}$ <p>FWHM of PSF<sub>III</sub> (intensity distribution at the focus of the microscope objective) in Z direction</p> <p>No influence by the pinhole</p>	<p>2. Axial resolution</p> $\frac{0.64 \bar{\lambda}}{(n - \sqrt{n^2 - NA^2})}$ <p>FWHM of total PSF in Z direction</p> <p>As optical slice thickness and resolution are identical in this case, depth resolution is often used as a synonym.</p>
<p>3. For comparison: FWHM of PSF in the intermediate image (Z direction) – referred to the object plane</p> $\frac{1.67 \cdot n \cdot \lambda_{em}}{NA^2}$	<p>3. Approximation to 2. for NA &lt; 0.5</p> $\frac{1.67 \cdot n \cdot \lambda_{exc}}{NA^2}$	<p>3. Approximation to 2. for NA &lt; 0.5</p> $\frac{1.28 \cdot n \cdot \bar{\lambda}}{NA^2}$
<p>4. Lateral resolution</p> $\frac{0.51 \cdot \lambda_{em}}{NA}$ <p>FWHM of the diffraction pattern in the intermediate image – referred to the object plane) in X/Y direction</p>	<p>4. Lateral resolution</p> $\frac{0.51 \cdot \lambda_{exc}}{NA}$ <p>FWHM of PSF<sub>III</sub> (intensity distribution at the focus of the microscope objective) in X/Y direction  <i>plus contrast-enhancing effect of the pinhole because of stray light suppression</i></p>	<p>4. Lateral resolution</p> $\frac{0.37 \cdot \bar{\lambda}}{NA}$ <p>FWHM of total PSF in X/Y direction  <i>plus contrast-enhancing effect of the pinhole because of stray light suppression</i></p>

All data in the table refer to quantities in the object space and apply to a fluorescent point object.

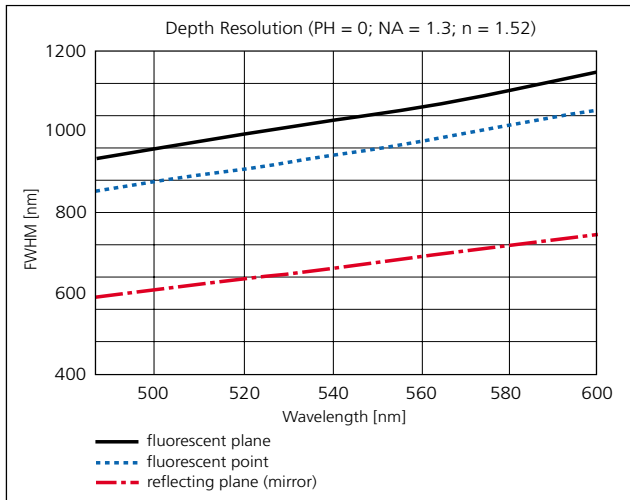
1) The equation is valid only for PH > 1 AU, i.e. transformation into the equation for PH = 0 by forming a limit (PH → 0) is not possible. PH < ∞ is meant to express a pinhole diameter of < 4.5 AU.



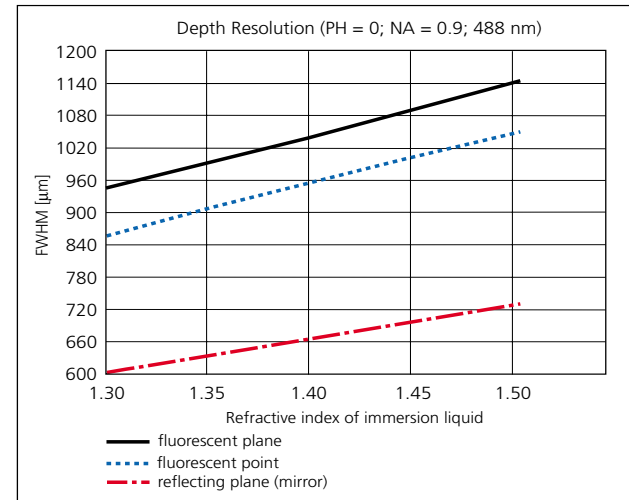
a) Variation of pinhole diameter



b) Variation of numerical aperture



c) Variation of wavelength



d) Variation of refractive index



# Electronic Signal Processing

## 1. Introduction

After the optical phenomena have been discussed in Part I, Part II takes a closer look at how the digitizing process and system-inherent sources of noise limit the system's performance.

As stated in Part I, a confocal LSM scans the specimen surface point by point. This means that an image of the total specimen is not formed simultaneously, with all points imaged in parallel (as, for example, in a CCD camera), but consecutively as a series of point images. The resolution obtainable depends on the number of points probed in a feature to be resolved.

Confocal microscopy, especially in the fluorescence mode, is affected by noise of light. In many applications, the number of light quanta (photons) contributing to image formation is extremely small. This is due to the efficiency of the system as a whole and the influences involved, such as quantum yield, bleaching and saturation of fluorochromes, the transmittance of optical elements etc. (see *InfoBox "Fluorescence"*). An additional influence factor is the energy loss connected with the constriction of the pinhole diameter.

In the following passages, the influences of scanning and noise on resolution are illustrated by practical examples and with the help of a two-point object. This is meant to be an object consisting of two self-luminous points spaced at 0.5 AU (see *InfoBox "Optical Coordinates"*). The diffraction patterns generated of the two points are superimposed in the image space, with maximum of one pattern coinciding with the first minimum of the other. The separate visibility of the points (resolution) depends on the existence of a dip between the two maxima (see Figure 8).

## 2. Digitization / Signal Processing

As a rule, object information is detected by a photomultiplier (PMT). The PMT registers the spatial changes of object properties  $I(x)$  as a temporal intensity fluctuation  $I(t)$ . Spatial and temporal coordinates are related to each other by the speed of the scanning process ( $x = t \cdot v_{\text{scan}}$ ). The PMT converts optical information into electrical information. The continuous electric signal is periodically sampled by an analog-to-digital (A/D) converter and thus transformed into a discrete, equidistant succession of measured data (pixels) (Figure 7).

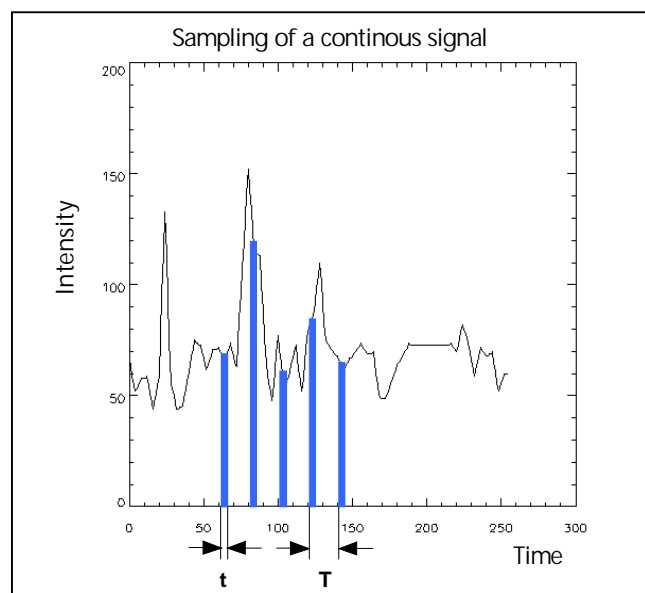


Fig. 7 Pointwise sampling of a continuous signal  
 $T$  = spacing of two consecutive sampling points  
 $t$  = time of signal detection ( $t \ll T$ )

The quality of the image scanned depends on the type of A/D conversion which is employed.

- Sampling: The time ( $t$ ) for signal detection (measurement) is small compared to the time ( $T$ ) per cycle (pixel time) (see Figure 7).
- Integration: The signal detection time has the same order of magnitude as the pixel time.

## Fluorescence

Fluorescence is one of the most important contrasting methods in biological confocal microscopy.

Cellular structures can be specifically labeled with dyes (fluorescent dyes = fluorochromes or fluorophores) in various ways. Let the mechanisms involved in confocal fluorescence microscopy be explained by taking fluorescein as an example of a fluorochrome. Fluorescein has its absorption maximum at 490 nm. It is common to equip a confocal LSM with an argon laser with an output of 15-20 mW at the 488 nm line. Let the system be adjusted to provide a laser power of 500  $\mu$ W in the pupil of the microscope objective. Let us assume that the microscope objective has the ideal transmittance of 100%.

With a C-Apochromat 63x/1.2W, the power density at the focus, referred to the diameter of the Airy disk, then is  $2.58 \cdot 10^5$  W/cm<sup>2</sup>. This corresponds to an excitation photon flux of  $6.34 \cdot 10^{23}$  photons/cm<sup>2</sup>sec. In conventional fluorescence microscopy, with the same objective, comparable lighting power (xenon lamp with 2 mW at 488 nm) and a visual field diameter of 20 mm, the excitation photon flux is only  $2.48 \cdot 10^{18}$  photons/cm<sup>2</sup>sec, i.e. lower by about five powers of ten.

This is understandable by the fact that the laser beam in a confocal LSM is focused into the specimen, whereas the specimen in a conventional microscope is illuminated by parallel light.

The point of main interest, however, is the fluorescence (F) emitted.

The emission from a single molecule depends on the molecular cross-section  $\sigma$ , the fluorescence quantum yield  $Q_e$  and the excitation photon flux as follows:

$$F = \sigma \cdot Q_e \cdot I \text{ [photons/sec]}$$

In principle, the number of photons emitted increases with the intensity of excitation. Actually, however, the limiting parameter is the maximum emission rate of the fluorochrome molecule, i.e. the number of photons emittable per unit of time. The maximum emission rate is determined by the lifetime (= radiation time) of the excited state. For fluorescein this is about 4.4 nsec (subject to variation according to the ambient conditions). On average, the maximum emission rate of fluorescein is  $2.27 \cdot 10^8$  photons/sec. This corresponds to an excitation photon flux of  $1.26 \cdot 10^{24}$  photons/cm<sup>2</sup>sec.

At rates greater than  $1.26 \cdot 10^{24}$  photons /cm<sup>2</sup>sec, the fluorescein molecule becomes saturated.

An increase in the excitation photon flux will then no longer cause an increase in the emission rate; the number of photons absorbed remains constant. In our example, this case occurs if the laser power in the pupil is increased from 500  $\mu$ W to roughly 1 mW. Diagram 5 shows the relationship between the excitation photon flux and the laser power in the pupil of the stated objective for a wavelength of 488 nm. Diagram 6 illustrates the excited-state saturation of fluorescein molecules. The number of photons absorbed is approximately proportional to the number of photons emitted (logarithmic scaling).

The table below lists the characteristics of some important fluorochromes:

	Absorpt.max.(nm)	$\sigma/10^{-16}$	$Q_e$	$\sigma^*Q/10^{-16}$
Rhodamine	554	3.25	0.78	0.91
Fluorescein	490	2.55	0.71	1.81
Texas Red	596	3.3	0.51	1.68
Cy 3.18	550	4.97	0.14	0.69
Cy 5.18	650	7.66	0.18	1.37

Source: Handbook of Biological Confocal Microscopy, p. 268 /Waggoner

In the example chosen,  $F = 1.15 \cdot 10^8$  photons/sec or 115 photons/ $\mu$ sec

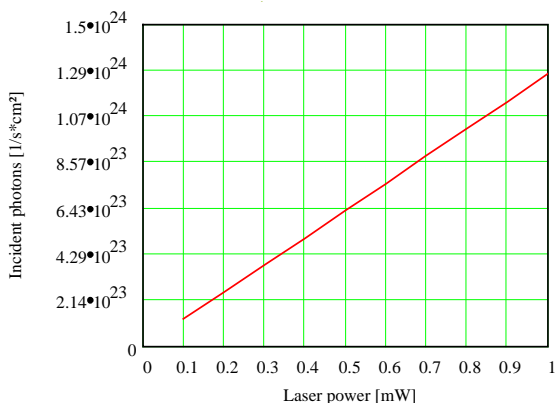


Diagram 5 Excitation photon flux at different laser powers

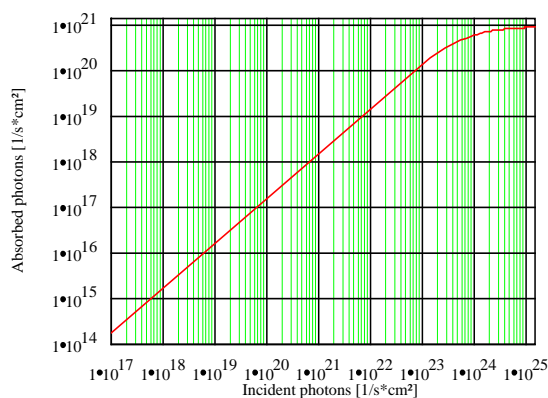


Diagram 6 Excited-state saturation behavior (absorbed photons) of fluorescein molecules

What has been said so far is valid only as long as the molecule is not affected by photobleaching. In an oxygen-rich environment, fluorescein bleaches with a quantum efficiency of about  $2.7 \cdot 10^{-5}$ . Therefore, a fluorescence molecule can, on average, be excited  $n = 26,000$  times ( $n = Q/Q_b$ ) before it disintegrates.

With  $t = \frac{n}{F_{\max}}$ , and referred to the maximum emission rate, this corresponds to a lifetime of the fluorescein molecule of about 115  $\mu$ s.

It becomes obvious that an increase in excitation power can bring about only a very limited gain in the emission rate. While the power provided by the laser is useful for FRAP (fluorescence recovery after photobleaching) experiments, it is distinctly too high for normal fluorescence applications. Therefore it is highly important, that the excitation power can be controlled to fine increments in the low-intensity range.

A rise in the emission rate through an increased fluorophore concentration is not sensible either except within certain limits. As soon as a certain molecule packing density is exceeded, other effects (e.g. quenching) drastically reduce the quantum yield despite higher dye concentration.

Another problem to be considered is the system's detection sensitivity. As the fluorescence radiated by the molecule goes to every spatial direction with the same probability, about 80% of the photons will not be captured by the objective aperture ( $NA = 1.2$ ).

With the reflectance and transmittance properties of the subsequent optical elements and the quantum efficiency of the PMT taken into account, less than 10% of the photons emitted are detected and converted into photoelectrons (photoelectron = detected photon).

In case of Fluorescein ( $NA = 1.2$ , 100  $\mu$ W excitation power,  $\lambda = 488$ ), a photon flux of  $F \sim 23$  photons/ $\mu$ sec results. In combination with a sampling time of 4  $\mu$ sec/pixel this means to 3-4 photoelectrons /molecule and pixel.

In practice, however, the object observed will be a labeled cell. As a rule, the cell volume is distinctly greater than the volume of the sampling point. What is really interesting, therefore, is the number of dye molecules contained in the sampling volume at a particular dye concentration. In the following considerations, diffusion processes of fluorophore molecules are neglected. The computed numbers of photoelectrons are based on the parameters listed above. With  $\lambda = 488$  nm and  $NA = 1.2$  the sampling volume can be calculated to be  $V = 12.7 \cdot 10^{-18}$  l. Assuming a dye concentration of 0.01  $\mu$ Mol/l, the sampling volume contains about 80 dye molecules. This corresponds to a number of about 260 photoelectrons/pixel. With the concentration reduced to 1 nMol/l, the number of dye molecules drops to 8 and the number of photoelectrons to 26/pixel. Finally it can be said that the number of photons to be expected in many applications of confocal fluorescence microscopy is rather small ( $< 1000$ ). If measures are taken to increase the number of photons, dye-specific properties, such as photobleaching, have to be taken into account.

Integration is equivalent to an averaging of intensities over a certain percentage of the pixel time known as pixel dwell time. To avoid signal distortion (and this to prevent a loss of resolution), the integration time must be shorter than the pixel time. The highest resolution is attained with point sampling (the sampling time is infinitesimally short, so that a maximum density of sampling points can be obtained). By signal integration, a greater share of the light emitted by the specimen contributes to the image signal. Where signals are weak (e.g. fluorescence), this is a decisive advantage over point sampling with regard to the signal-to-noise ratio (SNR). Therefore, Carl Zeiss confocal LSM systems operate in the integration mode, as a rule. The absolute integration time can be varied by varying the scanning speed, which also means a change of the pixel time. It is known from Part I that the information content of the signal is limited by the resolving power of the microscope optics. A realistic estimate for the resolving power is the full width at half intensity ( $FWHM_{lat}$ ) of a point image (see equation 3).

To avoid a loss of information during the scanning process, it is necessary to stick to the Nyquist theorem. The optimal pixel spacing in scanning a periodic signal, as defined by the Nyquist theorem, is half the period of the feature spacing to be resolved, or two pixels per resolvable structure detail. Together with the resolving power defined above this results in a maximum pixel spacing of  $d_{pix} = 0.5 \times FWHM_{lat}$ .

With a two-point object (see explanation on page 17), the pixel spacing needed to separate the two Airy discs in the digitized image is 0.25 AU (Figure 8).

If the number of sampling points per feature size is smaller than that given by the Nyquist theorem (undersampling), part of the information will be lost. This is evident in Figure 9c especially by the unresolved fine features.

A greater number of sampling points per feature size (oversampling) means a greater number of readings without a gain in information; simultaneously, the time per pixel becomes shorter. Thus, the volume of data to be processed is inflated, and the noise of the measurement signal increases (see section 3).

Under unfavorable conditions, also artifacts may result out of the digitization process (aliasing). As a rule, this is the case if the feature spacing in the specimen is equal, or nearly equal, to the pixel spacing.

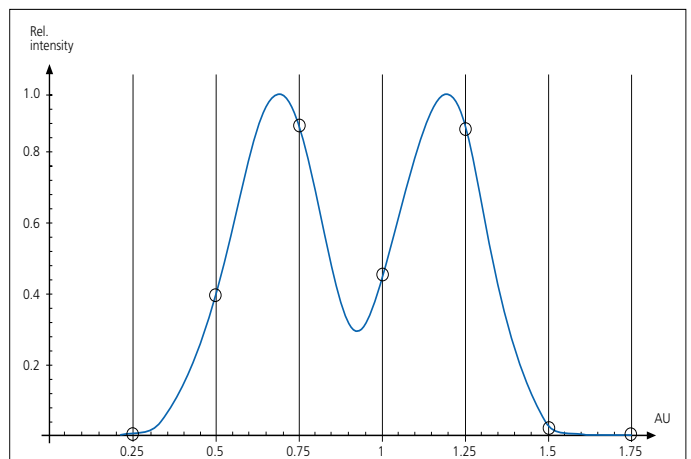


*Fig. 8 The graph illustrates the scanning of a two-point object with the minimum number of sampling points needed to avoid a loss of resolution (spacing of sampling points 0.25 AU).*

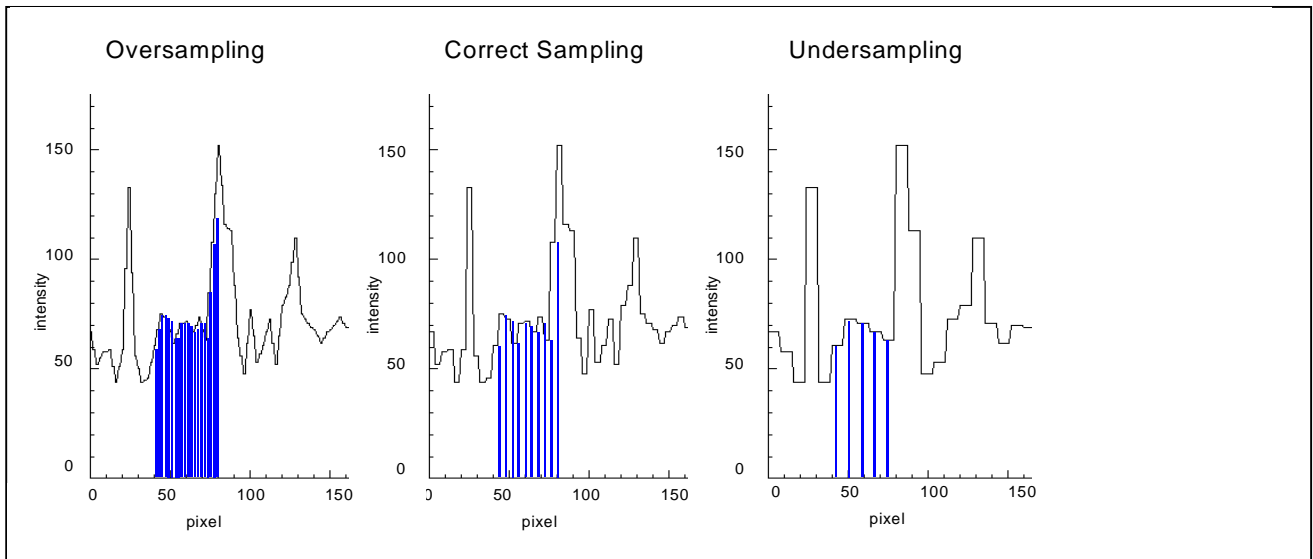


Fig. 9 Oversampling, correct sampling and undersampling of a continuous signal

A quantity of decisive importance in this connection is the maximum scanning angle set via the scanning zoom. By varying the scanning angle, it is possible to directly influence the edge length of the scanned field in the intermediate image plane (or object plane), and thus the physical pixel size (at a given number of pixels per line). The smaller the scanning angle, the smaller is the edge length of the scanned field, and the smaller is the pixel (see the example below).

In this way, the user of a Carl Zeiss confocal LSM can control the sampling rate (pixel size). For setting the suitable scanning zoom for correct Nyquist sampling, the pixel size  $d_{\text{pix}}$  in the object is important.

For a Carl Zeiss confocal LSM, there is a simple formula, based on the edge length of the scanned field in the intermediate image:

$$d_{\text{pix}} = \frac{\text{systemconst}}{\text{Number of Pixels} \cdot \text{Zoom factor} \cdot \text{Magnification}_{\text{obj}}}$$

Number of pixels = number of pixels per line,  
 Zoom factor (Z) = scanning zoom set in the software  
 (Example: Zoom factor 2 reduces the edge length of the scanned field by a factor of 2),  
 Magnification<sub>obj</sub> = objective magnification  
 system const. = 8.94 mm with LSM 510, LSM 5 Pascal (minimum zoom factor = 0.7); 12.77 mm with LSM 310, LSM 410 (minimum zoom factor = 1)

The minimum scanning zoom needed to fulfill the Nyquist theorem can therefore be calculated as follows:

$$Z \geq \frac{3.92 \cdot \text{NA} \cdot \text{systemconst}}{\text{Number of Pixels} \cdot \text{Magnification}_{\text{obj}} \cdot \lambda_{\text{exc}}}$$

NA = numerical aperture of objective  
 $\lambda$  = excitation wavelength

For example, with a 40x objective (NA = 1.3), 512 pixels per scan line and a wavelength of 488 nm, the full resolving power (correct sampling) is achieved with a scanning zoom of 4.56 as a minimum; the corresponding pixel size is 95.8 nm. With lower factors of the scanning zoom the pixel size itself will be the limiting factor for resolution (pixel resolution). Higher factors will cause oversampling. Hence, the zoom factor influences not only the total magnification but also the resolution properties of the system.

With the more recent LSM systems of Carl Zeiss, the number of sampling points can also be influenced by an increase in the number of pixels per scan line. (The number of pixels (X/Y) per image can be freely selected between 4 x 2 and 2048 x 2048).

### 3. Noise

The main factors of noise important in a confocal LSM system are detector noise (dark noise, secondary emission noise), laser noise, and shot noise of the light (see *InfoBox "Sources of Noise"*). As a rule, these sources of noise are of a statistical nature. Periodic noise occurs rarely ever, and if it does, it tends to correlate with defective devices or mechanical vibration in the setup; therefore it has been left out of consideration here.

As the illustration below (Figure 10) shows, the number of photons hitting the PMT depends not only on the intensity of fluorescence (see *InfoBox "Fluorescence"*), but also on the diameter of the pinhole. The graph shows the intensity distribution of a two-point object resulting behind the pinhole, in normalized (left) and non-normalized form (right). The pinhole diameter was varied between 2 AU and 0.05 AU. At a diameter of 1 AU the pinhole just equals the size of the Airy disk, so that there is only a slight loss in intensity. The gain in resolution, though, is minimum in this case.

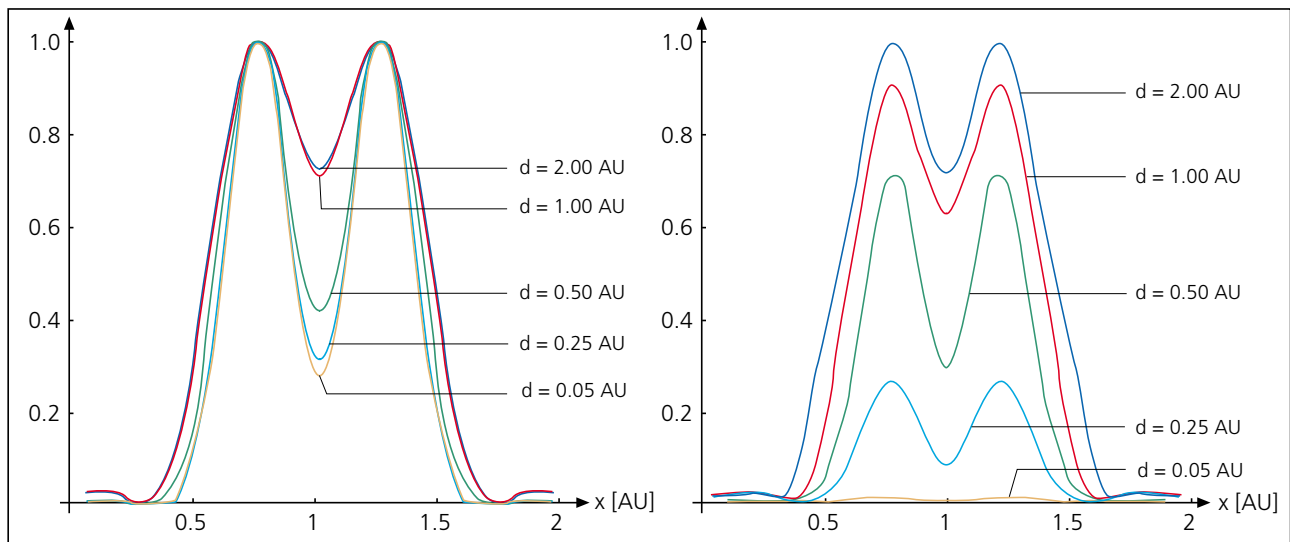
With a pinhole diameter  $< 1$  AU, resolution improves (better point separation thanks to a deeper dip), which is penalized by a drastic loss in energy.

Moreover, it should be considered that the question which noise source dominates depends on the signal level. With high-amplitude signals (number of detected photons  $> 10000$ ), laser noise is the dominating effect, whereas the quality of low signals (number of detected photons  $< 1000$ ) is limited by the shot noise of the light.

Therefore, laser noise tends to be the decisive noise factor in observations in the reflection mode, while shot noise dominates in fluorescence work. With recent PMT models (e.g., from Hamamatsu), detector dark noise is extremely low, same as secondary emission noise, and both can be neglected in most practical applications (see *InfoBox "Sources of Noise"*).

Therefore, the explanations below are concentrated on the influence of shot noise on lateral resolution.

*Fig. 10 As shown in Part I, small pinhole diameters lead to improved resolution (smaller FWHM, deeper dip - see normalized graph on the left). The graph on the right shows, however, that closing the pinhole is connected with a drastic reduction in signal level. The drop in intensity is significant from  $PH < 1$  AU ( $AU = AE$ ).*



**Sources of Noise**

Sources of noise effective in the LSM exist everywhere in the signal train - from the laser unit right up to A/D conversion. Essentially, four sources of noise can be distinguished:

**Laser noise q**

Laser noise is caused by random fluctuations in the filling of excited states in the laser medium. Laser noise is proportional to the signal amplitude N and therefore significant where a great number of photons (N < 10000) are detected.

**Shot noise (Poisson noise)**

This is caused by the quantum nature of light. Photons with the energy  $h \cdot \nu$  hit the sensor at randomly distributed time intervals. The effective random distribution is known as Poisson distribution. Hence,

$$SNR \approx \Delta N_{\text{Poisson}} = \sqrt{N}$$

where N = number of photons detected per pixel time (= photoelectrons = electrons released from the PMT cathode by incident photons). With low photoelectron numbers (N < 1000), the number N of photons incident on the sensor can only be determined with a certainty of  $\pm \sqrt{N}$ .

N can be computed as

$$N = \frac{\text{Photonen}}{QE(\lambda) \cdot \text{Pixeltime}}$$

where  $QE(\lambda)$  = quantum yield of the sensor at wavelength  $\lambda$ ; 1 photon =  $h \cdot c / \lambda$ ; c = light velocity; h = Planck's constant

**Multiplicative (secondary emission) noise**

Caused by the random variation of photoelectron multiplication at the dynodes of a PMT. The amplitude of multiplicative noise is a factor between 1.1 and 1.25, depending on the dynode system and the high voltage applied (gain). Generally, the higher the PMT voltage, the lower the secondary emission noise; a higher voltage across the dynodes improves the collecting efficiency and reduces the statistical behavior of multiplication.

**Dark noise**

Dark noise is due to the generation of thermal dark electrons  $N_d$ , irrespective of whether the sensor is irradiated.  $N_d$  statistically fluctuates about  $\sqrt{N_d}$ . Dark noise is specified for a PMT voltage of 1000 V; with lower voltages it progressively loses significance.

Dark noise can be reduced by cooling the sensor. However, the reduction is significant only if  $N \leq N_d$ , e.g. in object-free areas of a fluorescence specimen. In addition, the dark noise must be the dominating noise source in order that cooling effects a signal improvement; in most applications, this will not be the case.

Additional sources of noise to be considered are amplifier noise in sensor diodes and readout noise in CCD sensors. In the present context, these are left out of consideration. The mean square deviation  $\Delta N$  from the average (N + Nd) of the photoelectrons and dark electrons registered,

$$\Delta N = se \sqrt{(N + N_d)(1 + q^2)}$$

so that the total signal-to-noise ratio can be given as

$$SNR \approx \sqrt{\frac{N^2}{se^2 (N + N_d) (1 + q^2)}}$$

where

N number of photoelectrons per pixel time (sampling time),

se multiplication noise factor of secondary emission,

q peak-to-peak noise factor of the laser,

Nd number of dark electrons in the pixel or sampling time.

Example:

For N=1000, Nd=100, se=1.2, and q=0.05,

$$SNR \approx \sqrt{\frac{1000^2}{1.2^2 (1000 + 100) (1 + 0.05^2)}}$$

$$SNR \approx 25.1$$

### 3.1 Resolution and shot noise - resolution probability

If the number of photons detected ( $N$ ) is below 1000, fluorescence emission should be treated as a stochastic rather than a continuous process; it is necessary, via the shot noise, to take the quantum nature of light into account (the light flux is regarded as a photon flux, with a photon having the energy  $E = h \cdot \nu$ ). Resolution becomes contingent on random events (the random incidence of photons on the detector), and the gain in resolution obtainable by pinhole constriction is determined by the given noise level. Figure 11 will help to understand the quantum nature of light.

As a possible consequence of the shot noise of the detected light, it may happen, for example, that noise patterns that change because of photon statistics, degrade normally resolvable object details in such a way that they are not resolved every time in repeated measurements. On the other hand, objects just outside optical resolvability may appear resolved because of noise patterns modulated on them. Resolution of the "correct" object structure is the more probable the less noise is involved, i.e. the more photons contribute to the formation of the image. Therefore, let us talk of resolution probability rather than of resolution, and consider a model which combines the purely optical understanding of image formation in the confocal microscope (PSF) with the influences of shot noise of the detected light and the scanning and digitization of the object in view of the discernability of object details. Diagram 7 shows the dependence of the resolution probability on signal level and pinhole diameter by the example of a two-point object and for different numbers of photoelectrons/point object. If we consider that the image of a point objects is covered by a raster of pixels, a normalization based on pixels does not appear sensible.

Thus, a number of 100 photoelectrons/point object means that the point object emits as many photons within the sampling time as to result in 100 photoelectrons behind the light-sensitive detector target (PMT cathode). The number of photoelectrons obtained from a point object in this case is about twice the number of photoelectrons at the maximum pixel (pixel at the center of the Airy disk). With photoelectrons as a unit, the model is independent of the sensitivity and noise of the detector and of detection techniques (absolute integration time / point sampling / signal averaging). The only quantity looked at is the number of detected photons.

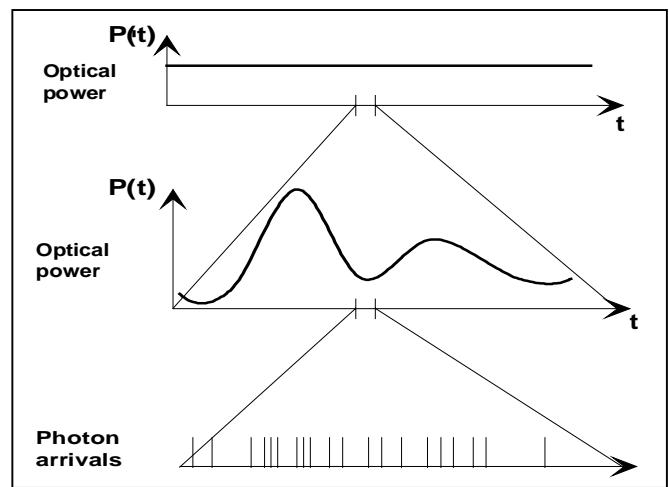


Fig. 11 The quantum nature of light can be made visible in two ways:  
a) by reducing the intensity down to the order of single photons and  
b) by shortening the observation time, despite high intensity.

The graph above illustrates case (b) – by diminishing the observation time, it is possible to resolve individual photons of the light flux in their irregular (statistical) succession.

A resolution probability of 90% is considered necessary for resolving the two point images. Accordingly, the two-point object defined above can only be resolved if each point produces at least about 25 photoelectrons. With pinhole diameters smaller than 0.25 AU, the drastic increase in shot noise (decreasing intensity of the detected light) will in any case lead to a manifest drop in resolution probability, down to the level of indeterminateness ( $\leq 50\%$  probability) at  $PH = 0$ .

As another consequence of shot noise, the curve maximum shifts toward greater pinhole diameters as the number of photoelectrons drops.

The general slight reduction of resolution probability towards greater pinhole diameters is caused by the decreasing effectiveness of the pinhole and the decline in the associated effects (suppression of out-of-focus object regions etc.; see Part I).

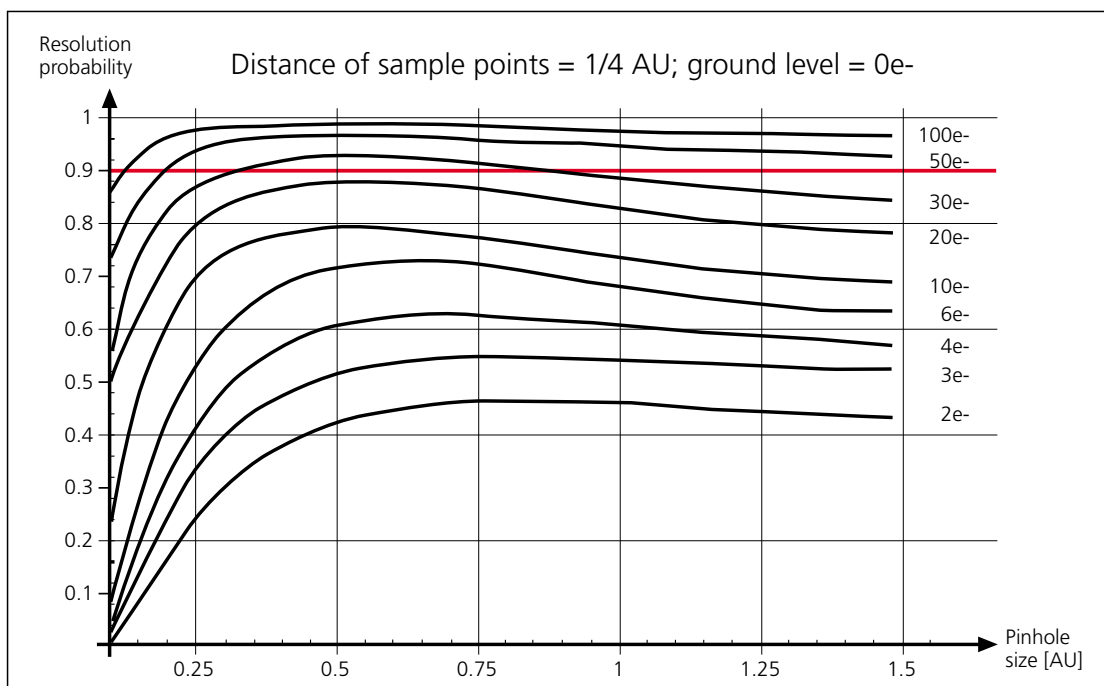


Diagram 7 The graph shows the computed resolution probability of two self-luminous points (fluorescence objects) spaced at  $1/2$  AU, as a function of pinhole size for various photoelectron counts per point object ( $e^-$ ). The image raster conforms to the Nyquist theorem (critical raster spacing =  $0.25$  AU); the image raster is subjected to interpolation. The photoelectron count per point object is approximately twice that per pixel (referred to the pixel at the center of the Airy disk). Each curve has been fitted to a fixed number of discrete values, with each value computed from 200 experiments.

The resolution probability is the quotient between successful experiments (resolved) and the total number of experiments. A resolution probability of 70% means that 7 out of 10 experiments lead to resolved structures. A probability  $> 90\%$  is imperative for lending certainty to the assumption that the features are resolved. If we assume a point-like fluorescence object containing 8 FITC fluorescence molecules (fluorochrome concentration of about  $1$  nMol) a laser power of  $100 \mu\text{W}$  in the pupil and an objective NA of  $1.2$  ( $n = 1.33$ ), the result is about  $45$  photoelectrons / point object on the detection side.

The pinhole diameter selected in practice will therefore always be a trade-off between two quality parameters: noise (SNR as a function of the intensity of the detected light) and resolution (or depth discrimination). The pinhole always needs a certain minimum aperture to allow a minimum of radiation (depending on the intensity of fluorescence) to pass to the detector.

Where fluorescence intensities are low, it may be sensible to accept less than optimum depth discrimination so as to obtain a higher signal level (higher intensity of detected light = less noise, better SNR). For most fluorescent applications a pinhole diameter of about 1 AU has turned out to be the best compromise.

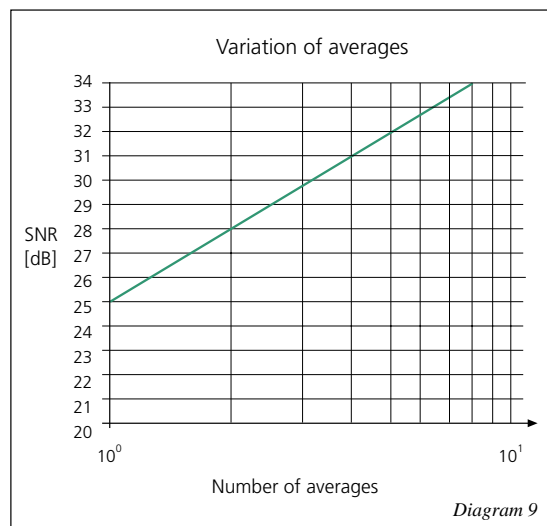
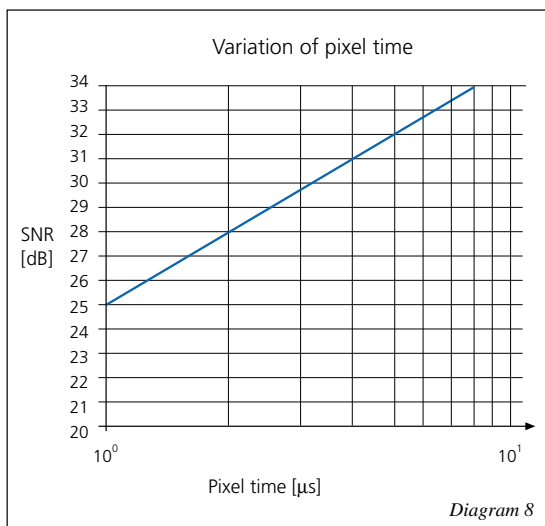
### 3.2 Possibilities to improve SNR

Pinhole diameters providing a resolution probability below 90% may still possibly yield useful images if one uses a longer pixel time or employs the signal averaging function. In the former case, additional photons are collected at each pixel; in the latter case, each line of the image, or the image as a whole, is scanned repeatedly, with the intensities being accumulated or averaged. The influence of shot noise on image quality decreases as the number of photons detected increases. As fluorescence images in a confocal LSM tend to be shot-noise-limited, the increase in image quality by the methods described is obvious.

With these methods, detector noise is also reduced, same as laser noise at high signal levels. The diagrams below show the influence of pixel time (Diagram 8) and the influence of the number of signal acquisitions (Diagram 9) on SNR in [dB]. The linearity apparent in the semilogarithmic plot applies to shot-noise-limited signals only. (As a rule, signals are shot-noise-limited if the PMT high voltage needed for signal amplification is greater than 500 V).

A doubling of pixel time, same as a doubling of the number of signal acquisitions, improves SNR by a factor of  $\sqrt{2}$  (3 dB). The advantage of the averaging method is the lower load on the specimen, as the exposure time per pixel remains constant. Photon statistics are improved by the addition of photons from several scanning runs ( $SNR \approx \sqrt{n \cdot N}$ ;  $N = \text{const.}$ ,  $n = \text{number of scans averaged}$ ). By comparison, a longer pixel time directly improves the photon statistics by a greater number  $N$  of photons detected per pixel ( $SNR \approx \sqrt{N}$ ,  $N = \text{variable}$ ), but there is a greater probability of photobleaching or saturation effects of the fluorophores.

*Diagrams 8 and 9 Improvement of the signal-to-noise ratio. In Diagram 8 (left), pixel time is varied, while the number of signal acquisitions (scans averaged) is constant. In Diagram 9 (right), pixel time is constant, while the number of signal acquisitions is varied. The ordinate indicates SNR in [dB], the abscissa the free parameter (pixel time, scans averaged).*



The pictures below demonstrate the influence of pixel time on SNR; object details can be made out much better, if the pixel time increases.

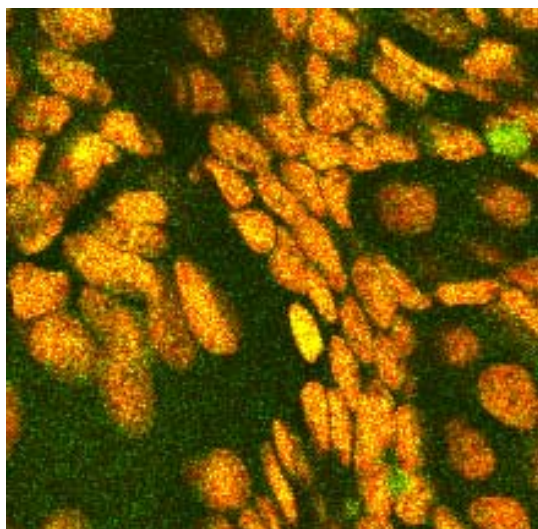
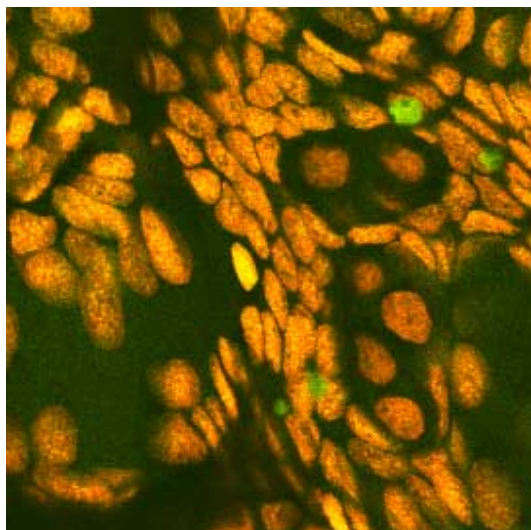


*Fig. 12 Two confocal images of the same fluorescence specimen (mesophyll cells). Both images were recorded with identical parameters except pixel time, which is 4.48  $\mu$ s for the top image and 1.12  $\mu$ s for the bottom image. According to Diagram 8, the difference in SNR is 6 dB. The same effect can be observed if the averaging method is applied.*

Another sizeable factor influencing the SNR of an image is the efficiency of the detection beam path. This can be directly influenced by the user through the selection of appropriate filters and dichroic beamsplitters. The SNR of a FITC fluorescence image, for example, can be improved by a factor of about 4 (6 dB) if the element separating the excitation and emission beam paths is not a neutral 80/20% beamsplitter but a dichroic beamsplitter optimized for the particular fluorescence.

## 1. Summary

This monograph comprehensively deals with the quality parameters of resolution, depth discrimination, noise and digitization, as well as their mutual interaction. The set of equations presented allows in-depth theoretical investigations into the feasibility of carrying out intended experiments with a confocal LSM.

The difficult problem of quantifying the interaction between resolution and noise in a confocal LSM is solved by way of the concept of resolution probability; i.e. the unrestricted validity of the findings described in Part I is always subject to a sufficient number of photons reaching the detector.

Therefore, most applications of confocal fluorescence microscopy tend to demand pinhole diameters greater than 0.25 AU; a diameter of 1 AU is a typical setting.

## Authors / Sources / References

### Authors:

(on the R&D staff of Carl Zeiss Jena)

Stefan Wilhelm,  
Bernhard Gröbler,  
Martin Gluch,  
Hartmut Heinz †,

We gratefully acknowledge the assistance of many other Carl Zeiss Jena staff members who contributed to this brochure.

1. Barton, D.L., Tangyonyong, P., Scanning Fluorescent Microthermal Imaging, Proceedings of 23<sup>rd</sup> Int Symposium for Testing and Failure Analysis (10/1997), Santa Clara, California
2. Barton, D.L., Tangyonyong, P., Infrared Light Emission from Semiconductor Devices, ISTFA, pp. 9-17, (1996)
3. Beyer, H.: Handbuch der Mikroskopie, 2nd Edition, VEB Verlag Technik Berlin, (1985)
4. Brismar, H., Trepte, O., Ulfhake, B.: Spectra and Fluorescence Lifetimes of Lissamine, Rhodamine etc....: Influences of Some Environmental Factors Recorded with a Confocal Laser Scanning Microscope, The Journal of Histochemistry and Cytochemistry, Vol. **43**, pp. 699-707, (7/1995)
5. Keller, H.E., Objective Lens for Confocal Microscopy, Handbook of Biological Confocal Microscopy, pp. 111-125, Plenum Press, 2<sup>nd</sup> Edition (1995)
6. Lackmann, F., et. al., An Automated Latch-up Measurement System Using a Laser Scanning Microscope, SPIE Vol **1028** Scanning Imaging, (1988)
7. Gröbler, B., Untersuchungen zur Bildübertragung in abtastenden Mikroskopen unter besonderer Berücksichtigung der 3D-Abbildung, PhD thesis, University of Potsdam, (1995)
8. Hell, S., et al., Aberrations in confocal fluorescence microscopy induced by mismatches in refractive index, Journal of Microscopy, Vol. **169**, pp. 391-405 (3/1993)
9. Nitschke, R., Wilhelm, S., et al., A modified confocal laser scanning microscope allows fast ultraviolet ratio imaging of intracellular Ca<sup>2+</sup> activity using Fura 2, Euro. J. Physiologie, Vol. **433**: pp. 653-663, (1997)
10. Oldenbourg, R. et al., Image sharpness and contrast transfer in coherent confocal microscopy, Journal of Microscopy Vol. **172**, pp. 31-39, (10/1993)
11. Pawley, J., Handbook of Biological Confocal Microscopy, Plenum Press, 2<sup>nd</sup> Edition (1995)
12. Stelzer, E.H.K., The intermediate optical system of laser scanning confocal microscopes ; Handbook of Biological Confocal Microscopy, pp. 139-154, Plenum Press, 2<sup>nd</sup> Edition (1995)
13. Stelzer, E.H.K., et. al., Nondestructive sectioning of fixed and living specimens using a confocal scanning laser fluorescence microscope: Microtomoscopy; SPIE, Vol. **809**, pp. 130-136, (1987)
14. Tanke, H.J., van Oostveldt, P., et al., A parameter for the distribution of fluorophores in cells derived from measurements of inner filter effect and reabsorption phenomenon, Cytometry Vol. **2**, pp. 359-369 (6/1982)
15. Tsien, R.Y., Waggoner, A., Fluorophores for Confocal Microscopy , Handbook of Biological Confocal Microscopy, pp. 267-277, Plenum Press, 2<sup>nd</sup> Edition (1995)
16. Webb, R.H., Dorey, C.K., The Pixelated Image, Handbook of Biological Confocal Microscopy, pp. 55-66, Plenum Press, 2<sup>nd</sup> Edition (1995)
17. Wilhelm, S., Über die 3-D Abbildungsqualität eines konfokalen Laser Scan Mikroskops, Dissertation, Fachhochschule Köln, (1994)
18. Wilson, T., Carlini, A.R., Three dimensional imaging in confocal imaging systems with finite sized detectors; Journal of Microscopy, Vol. **149**, pp. 51-66, (1/1988)
19. Wilson, T., Carlini, A.R., Size of detector in confocal imaging systems; Optical Letters Vol. **12**, pp. 227-229, (4/1987)
20. Wilson, T., Sheppard, C. J.R., Theory and Practice of Scanning Optical Microscopy, Academic Press, 2<sup>nd</sup> Edition (1985)